THE UNIVERSITY OF QUEENSLAND

BACHELOR OF ENGINEERING THESIS

Energy Absorption in Woven Fibers Due to Engineered Fiber Undulation

Student Name: Channa MADUGALLE

Course Code: MECH4500

Supervisor: Dr Michael Hietzmann

Submission Date: 27 October 2017

A thesis submitted in partial fulfilment of the requirements of the
Bachelor of Engineering Degree in Mechanical and Aerospace Engineering

UQ Engineering

Faculty of Engineering, Architecture and Information Technology

Acknowledgments

To my loving parents and sister. I may never express it, but without you all, I would be nothing but a pile of dust.

To Dr Hietzmann for your trust and guidance. When we first started, this project sounded pretty boring. Nearly a year later, it has morphed to be one of the most exciting thesis projects anyone could undertake.

To Veronica Pajnic and Stephen 'Sami' Joseph for the heavy carry. Not only did you two push me over the line, you also made the journey memorable.

Abstract

This study discusses an investigation into determining whether the energy absorption properties of fibre-based armour systems could be manipulated through fibre undulations. The background context to the problem has been introduced along with a literature review on ballistic impact dynamics, existing armour systems and the gaps in the industry. Proof of concepts were developed using an iterative process to validate the performance of different undulation designs using both glass and Aramid fibre.

Mechanical testing was conducted to ascertain the material properties of the various followed by low-velocity ballistic impact testing. The impact testing was conducted using the pneumatic cannon commissioned by the Univeristy of Queensland's Composites Group to conduct impact testing.

A detailed analysis was conducted on the performance of each undulation design and a method was developed to quantify the performance of undulating designs.

Contents

List of Figures

List of Tables

Nomenclature

P_{max} = load at moment of failure

σ_b = flexural stress

E_b = flexural modulus

E_c = composite modulus

E_f = fibre modulus

E_m = matrix modulus

L = support span

b = width of beam tested

d = depth of beam tested

m = slope of the tangent to the initial straight-line

1 Introduction

A modern battle field is unprecedented in its nature. The ascent of asymmetrical threats for law enforcement and conventional militaries have driven significant research and investment into ballistic protection systems. Since the development of synthetic fibre nylons and subsequent body armour technologies in the 1940s, fibre based materials have dominated ballistic protection[20]. A high level of ballistic resistance and lightweight are at the forefront of the considerations for body armour. Furthermore, the same piece of armour is expected to perform in extremely rugged conditions ranging from hot humid summer conditions to snowy winter conditions [10].

2 Thesis Definition

With a modern soldier having to carry up to seventy kilograms of load, minimising the weight of body armour is critical to their manoeuvrability and survivability. Therefore, reducing the weight of an armour system requires an increase in the energy absorption properties in order to remain viable.

The National Institute of Justice (NIJ), the governing body for armour testing states that the current challenge is to increase comfort to the wearer without reducing ballistic resistance. Material research has been at the forefront of armour innovation. However, as expressed by Behera and Dash [2] in their study into mechanical behaviour of 3D composites, as limits are reached in the specific strength and moduli of fibres and matrix materials, a deeper level of understanding needs to be gained how fabric architectures affect and control the mechanical performance of laminates needs to be gained.

2.1 Aims

This study explores a methodology which attempts to increase the energy absorption of a fibre based material through the manipulation of the fibre architecture. By altering the fibres to form undulations, this study aims to determine the effects of the energy absorption properties of the material. If the engineered composite elements presents favourable results, further development into the theory will be considered.

2.2 Objectives

The objectives into this study have been summarised in the following order.

1. Critically analyse ballistic impact dynamics (penetration mechanisms) and the subsequent design considerations for composite armour elements.
2. Analyse the influence of the geometrical arrangement of fibres and its effects on energy absorption
3. Design, manufacture and test a proof of concept exploring fibre undulation theory
4. Detail recommendations for further research into this field of study in order to maximise the impact of the work conducted.

2.3 Scope and Research Focus

The field of ballistic protection is highly complex in nature. Therefore, in order achieve the research objectives while minimising the complexity, Table1 details the scope of this study.

Table 1: Scope of Study

In Scope	**Out of Scope**
• Hard armour plates (HAP) • Ballistic impacts involving small arms ammunition (strain rates between 10^{-2} and 10^{6})	• Material effects on energy absorption • Flexible body armour • Spike, knife and chemical energy threats • Effects due to shock physics omitted as only considering small arms ammunition [14]

It must be noted that this study did not focus on the effects of material selection on energy absorbability. The primary research focus was on the energy absorption due to fibre undulations using a simulated ballistic impact scenario.

2.4 Contributions Made By this Thesis

This thesis makes a key contribution to the area of armour materials. It introduces a novel and improved technique to manipulating the energy-absorption in fibre-reinforced laminated materials. Specifically, it develops a fundamental understanding of the energy absorption effects of composite laminates due to ply undulations in low velocity ballistic events.

3 Literature Review

3.1 The Threat, A Brief Background

The increased lethality of firearms and the occurrences of high-velocity fragmentation has forced ballistic protection to evolve to tailor-made armour systems combating specific threats. By analysing injuries sustained during past major conflicts, the reader is able to distinctly identify a sharp shift in the type of threat [7].

As highlighted by Brady, injuries sustained during the Vietnam war were predominantly due to close-quarter small arms fire or booby traps. Data collected by the Wound Data and Munitions Effectiveness Team (WDMET) from July to September 1967 highlighted that 50% of all casualties occurred at a range of under 10 m [3].

Operation Desert Storm (Iraq 1991) brought forth armour warfare in a desert environment. An analysis conducted into the casualties admitted to US Army Seventh Corps hospitals between 20 February and 10 March 1991 highlighted an increased number of casualties due to fragmentation. Of the 143 admitted, 136 were due to fragmentation. There were only seven injuries due to gunshot wounds admitted during this period [5].

Furthermore, Kelly et. al [16] conducted an analysis into the injuries and causes of death during Operation Iraqi Freedom (OIF, 2003-2004) and Operation Enduring Freedom (OEF, 2006). During OIF, out of 496 casualties analysed, 30% were due to gunshot wounds whereas 55% were from explosions. These explosions accounted for improvised explosive devices, fragmentation grenades, mines and artillery shells. In stark contrast, during OEF, out of the 501 casualties analysed, 24% were from gunshot wounds compared to the 76% from explosions.

Hence, this change in the nature of modern warfare has forced engineers to deeply consider high-velocity fragmentation when designing body armour. As highlighted by Crouch, the

unpredictability of various sized fragmentation travelling up to two thousand meters per second is a complex nexus that is difficult to model and design against. Therefore, current body armour testing standards primarily consider small-arms ammunition. While it is common to expect small-arms threats in battle-fields, it poses a considerable threat to law enforcement as well. Data collected in 2009 by the London Metropolitan Police showed that the specific deployment of ballistic protection by personnel was required for approximately 20% of their call-outs [10].

In small-arms ammunition the ballistic impact dynamics and penetration mechanisms are similar regardless of calibre. A bullet derives its penetrative power from its core. The weight, material and shape of the core determines the bullet's effectiveness. There are five specific bullet types used for the testing of ballistic performance. Table 2 presents a comparison of these bullet types.

Table 2: Bullet Types Used For Ballisitic Protection Testing [4]

Bullet Type	**Core**	**Description**
Semi-Jacketed Hollow Point (SJHP)		Lead-based core, heavy expansive bullet (mushrooms on impact).
Jacketed Soft Point (JSP)		Lead-based exposed core. Expansive bullet. Exposed core increases penetration. Commonly used for hand guns. Penetrative due to exposed core.
Full Metal Jacket (FMJ)		Lead-based core. Highly penetrative, non-expansive. Common military rifle round. Flat and round nose versions are common handgun ammunition.
Armour Piercing (AP)		Typical core materials include tungsten and hardened steel. Heavy, high-velocity round. Extremely penetrative due to hard-metal core.

3.2 Ballistic Protection Performance Standards

The governing document for standardised testing of ballistic protection is the National Institute of Justice Standard 0101.06, Ballistic Resistance of Body Armour (NIJS). This standard outlines a ballistic system's minimum performance requirements against varying threats. Furthermore, it details precise testing methods for the evaluation of the armour systems.

The NIJS classifies body armour using five separate types. These types are based on ballistic performance to different small arm calibres. Each body armour sample is tested at a undamaged state as-well-as at a *conditioned* state. This conditioned state is intended to simulate the armour's performance following exposure to specified levels of heat, moisture and mechanical damage. Therefore, the testing authority is able to simulate the operating conditions of the armour in combat. An outline of these categories are presented in Table 3.

Table 3: Armour Performance Levels as per NIJS-0101.6 [18]

Armour Type	**Bullet Calibre**	**Weight (g)**	**Velocity (m/s)**		**Maximum Impact Energy (J)**[1]
			Undamaged Panel	**Conditioned Panel**	
IIA	9 mm FMJ RN	8	373 ± 9.1	355 ± 9.1	584
	.40 in FMJ	11.7	353 ± 9.1	325 ± 9.1	767
II	9 mm FMJ RN	8	398 ± 9.1	379 ± 9.1	663
	.357 in JSP	10.2	436 ± 9.1	408 ± 9.1	1010
IIIA	.357 in FMJ FN	8.1	448 ± 9.1	430 ± 9.1	846
	.44 in SJHP	15.6	436 ± 9.1	408 ± 9.1	1545
III	7.62 mm FMJ	9.6	847 ± 9.1	847 ± 9.1	3518
IV	.3 in AP	10.8	878 ±9.1	878 ± 9.1	4250

To place the energy levels to context, a human punch ranges anywhere between 70-900 J depending on the weight and speed of the arm [**?**]. By definition, levels II and IIA pertain to law enforcement. Current standard issue military body armour is tested to level IIIA, capable of withstanding rifle fire. Level IV is designed to defeat armour-piercing projectiles. It is relevant to note that military armour (type III and IV) is expected to perform to the same standard for both as-new and conditioned states.

[1] calculated using the initial velocity of the round from the barrel

3.2.1 NIJ Testing Methodologies

Two different types of ballistic tests are utilised to evaluate the armour's performance. The first is the perforation and backfire signature test (P-BFS). This evaluates the amour's performance against blunt force trauma and perforation. As displayed in Figure 1, the panel is mounted against a backing material constructed from clay. The clay captures and records the backfire signature created during non-perforating impacts. Table 4 details the performance requirements necessary for each armour category. During this test, if a single round fully perforates the panel, the panel is deemed to fail. Furthermore, the backfire signature measured on the clay backing material must be less than 44 mm.

Table 4: Perforation and Backfire Signature Test Performance Requirements

Armour Type	**Test Bullet**	**Hits Per Panel at 0°**	**Hits Per Panel at 30°or 45°Angle**	**Maximum BFS Depth (mm)**
IIA	9 mm FMJ RN	4	2	44
	.40 in S&W FMJ	4	2	44
II	9 mm FMJ RN	4	2	44
	.357 in Magnum JSP	4	2	44
IIIA	.357 in SIG FMJ FN	4	2	44
	.44 in Magnum SJHP	4	2	44
III	7.62 mm FMJ	6	0	44
IV	.3 in AP	1-6	0	44

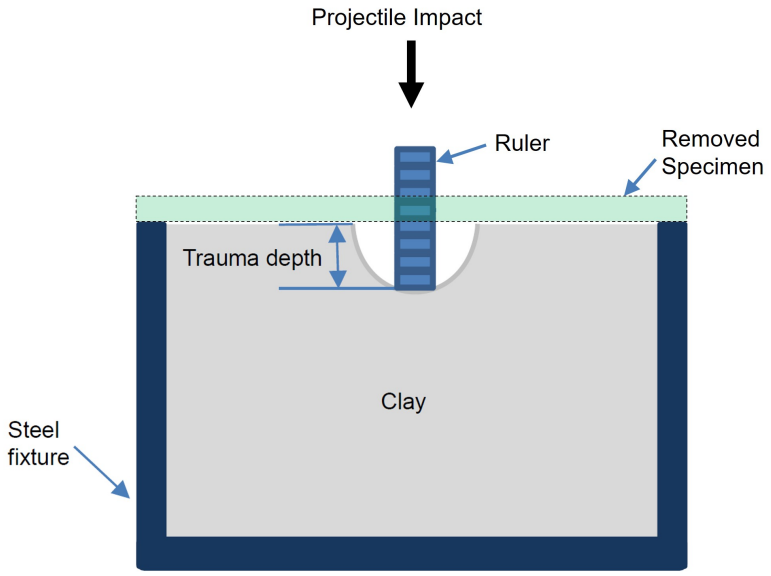

Figure 1: P-BFS Test Setup [18]

The second type of testing conducted on the armour are ballistic limit determination tests (BL), which estimates its ballistic performance. The tests are conducted on multiple panels with each panel having to withstand a minimum number of impacts. If a panel is not rated for the standard number of multiple hits for the threats defined in Table 3, multiple panels may be used to complete the test. Table 5 details the ballistic test performance requirements for each armour type.

Table 5: Ballistic Limit Test: Performance Requirements

Armour Type	**Minimum Shots Per Test**	**Minimum Shots Per Test Panel**	**Minimum Penetration Result (Full Test)**
II, IIA and IIIA	120	12	At least 60 stops At least 30 perforations
III	24	12[2]	6 perforations, 12 stops, velocity range $\pm$ 27m/s
IV	12	12[1]	3 perforations, 6 stops, velocity range $\pm$ 27m/s

Further to these performance requirements, the testing velocity for subsequent projectiles after the first are varied. Table 6 details the variation of this projectile velocity depending on the nature of the previous impact.

Table 6: Ballistic Limit Test: Velocity Variation

Description	**Velocity Magnitude Variation**
Velocity of first shot	As per Table 3
Velocity step until first reversal	$-$ 30.5 m/s if first shot perforated $+$ 30.5 m/s if first shot was stopped
Velocity step until a second reversal	$\pm$ 22.9 m/s, depending result of previous shot
Velocity step after second reversal	$\pm$ 15.2 m/s, depending result of previous shot

As stated before, the armour is tested for both as-new and conditioned states. In order to achieve the conditioned state, the armour is exposed to uniform thermal exposure conditions. For this, armour is exposed over a ten day period at 65°C and at 80% relative humidity. Mechanical

[2]or to the multi-hit limit rating as per the manufacturer

durability is tested via drop tests and the performance of the armour in submerged conditions are also tested for (minimum 30 minutes at 100 mm $\pm$ below water surface).

It is evident that ballistic armour undergoes rigorous technical testing prior to being rated against a specific threat. To ensure that the armour is designed sufficiently to these standards, a strong understanding of ballistic impact dynamics and energy absorption is imperative.

3.3 Ballistic Impact Dynamics

Compared to common quasistatic mechanical processes, ballistic impact dynamics is highly complex in nature [7]. The high-velocity impact event from the transverse direction is typically completed within one-hundred microseconds [10]. The generation and transmission of stress waves is critical to the analysis of the ballistic impact dynamics. The projectile strike causes the armour material to generate elastic, plastic or shock waves. The type of waves generated depends on the stress level involved.

Within the elastic regime, as expressed in equation 1, the stress waves are a function of bulk density and elastic modulus.

$$V = \sqrt{\frac{E}{\rho}} \tag{1}$$

Therefore, a decrease in the bulk density and increase in elastic modulus causes the velocity of the propagating wave to increase. This poses a significant issue for most fibre based composite materials with high elastic modulus and low bulk density. Upon impact, the stress wave generated moves faster than the impacting projectile which may cause the material ahead to be altered reducing ballistic performance of the material [10].

Focussing on individual tows, Figure 2 displays the propagation of stress waves and transverse waves of a single tow on impact. On impact, the tow compresses in the through- thickness direction initiating a transverse deflection as it is stretched forwards with the projectile [6]. A longitudinal wave travelling axially then builds up simultaneously and propagates away from the impact centre at the velocity of the sound in the material (c). This dissipates the energy away from the impact centre. Therefore, the elastic wave speed, expressed by the speed of sound in the material for a semi-infinite medium is expressed in equation 2. In a semi-infinite medium, the wave speed is a function of the Poisson's ratio (ν), elastic modulus and density of

the material [14].

$$c = \sqrt{\frac{E(1-\nu)}{\rho(1+\nu)(1-2\nu)}} \tag{2}$$

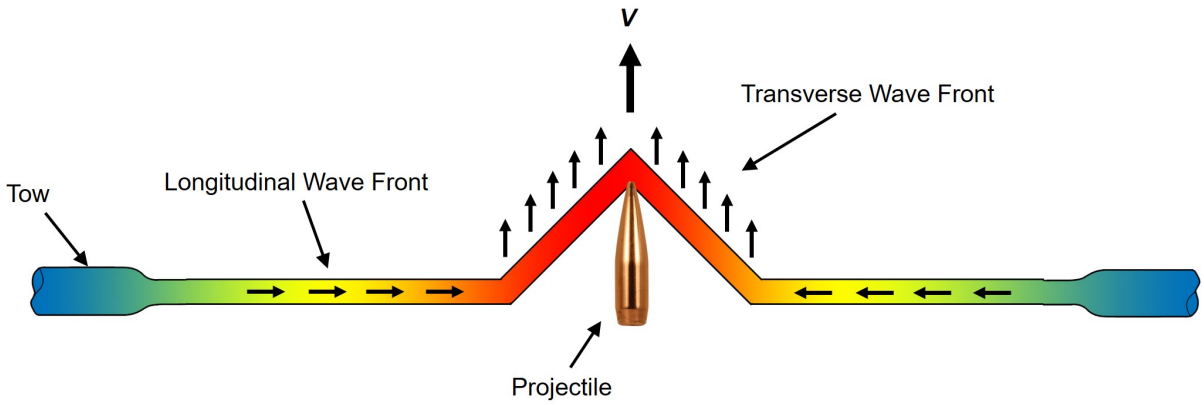

Figure 2: Stress and Transverse Wave Propagation Upon Ballistic Impact in Fibre Tow [18]

However, the elasticity of the fibre causes this wave to reflect back towards the impact centre once it reaches the panel's restrained ends. Furthermore, this inward movement causes the transverse deflection to compound. This process repeats until the strain experienced in the tow reaches breaking strain [7].

This feeds into a critical material characteristic which is the strain-rate sensitivity. The mechanical response of a material is sensitive to the rate at which it is loaded. Due to these time-dependant properties, the materials properties such as the elastic modulus may depend on the rate at which it is impacted.

However, there is limited information regarding the effects of high strain rates on fibrous composites. The non-homogeneous deformation of fibrous materials from stress waves has caused the quantification of force and deflection at high strain rates challenging. Gilat et al. [12] conducted a study into the strain rate sensitivity of carbon fibre and epoxy composite panels between 1 and 400 s^{-1} . At these intermediate strain rates, the stress-strain curves and the maximum stress of the materials were significantly affected. It was found that the laminates displayed a distinct strain rate sensitivity when their deformation was dominated by the shear in the resin. To accurately simulate small-arms fire strain rates, Crouch [10] states that a strain rate between 10^0 and- 10^4 s^{-1} needs to be achieved. For this range, the material responds adiabatically and at a plane stress state.

3.4 Energy Absorption

Cavallaro [6] discusses that the energy absorbability of woven fabrics to be dependant on its ability to restrict and enable tow motions within the weave. These motions are characterised by tow-to-tow interactions. A primary interaction concerning energy absorption is crimp interchange. Consider a plain-weave fabric under biaxial tension along the warp tows; the tension causes the warp tows to decrease crimp heights, stretch and attempt to straighten. The opposite happens to the weft tows where increase crimp heights, compress and reduce their effective length. This coupling effect is known as crimp interchange.

If the biaxial tension increases, tow kinematic (slip) at the tow crossover regions ceases and the spacing between the tows converge to a minimum, this phenomenon is referred to as the extensional-jamming point. It prevents the family of tows from straightening and not achieving its full strength [15].

Now, consider the same plain-weave fabric loaded uniaxially $\pm 45°$to the fibre direction. This shear loading causes the tow families to rotate at the cross-over regions. As the loading increases, the angle between the tows change due to the increased skewness between the tows. At large shear loadings, a phenomenon called shear jamming occurs. Here, the available space between the tow families decreases and rotational locking of the tow families occur [15]. The shear jamming angle decreases as the tow count increases per unit length. Loading beyond the onset of locking causes localised out-of-plane deformations.

Further, at crossover regions, friction between the tows minimise tow migrations away from the impact centre. As highlighted by Duan et al, an increased tow-to-tow friction coefficient provides increases in dynamic energy absorption capacities.

In an analysis conducted by Cunniff into system effects in woven fabrics under ballistic impact, it was highlighted that in multilayer armour, the ballistic energy absorbability does not scale with the energy absorption capacities of individual layers. This is due to the compressive stress of the primary tows (tows which directly in contact with projectile impact) in stacked fabrics exceeding the stresses in a single layer impact.

Hence the energy absorbability in multilayer systems will be discussed in the following section.

3.5 Penetration Mechanisms and Design Considerations

In multilayer armour, the impact failure modes need to be analysed to evaluate the necessary design considerations to suppress them. The primary failure modes in laminated armour as highlighted by Crouch are discussed in Table 7.

Table 7: Multilayer Armour Failure Modes [10]

Failure Mode	Description
Delamination 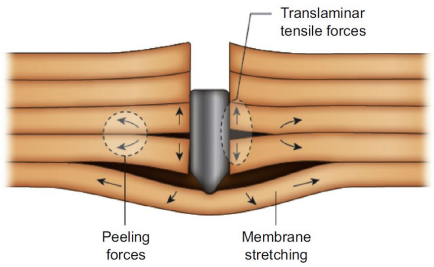	Delamination is the primary failure mode in laminated materials followed by through-thickness compression of impact. The primary energy absorbing mechanisms in this mode are membrane stretching (out-of-plane plastic deformation) and interlaminar fracture (either through translaminar tensile failure or interlaminar shear failure of bond).
Discing 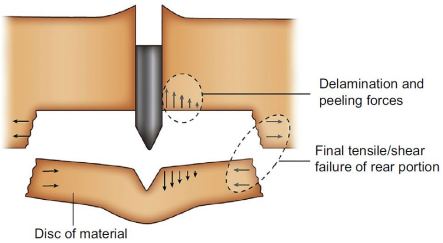	Discing is commonly observed following delamination and is a low-energy absorbing failure mode. Discing causes rear-face spalling in the target through high-velocity impact. It causes significant bending stress in the target initiating interlaminar shear cracks. Rapid propagation of these delamination cracks cause the separation of a disc through in-plane tensile-tearing fracture. Mode occurs late in penetration process.
Radial and Circumferential Cracking 	Typical failure modes observed in brittle materials. On impact, following conoidal fracture, radial cracks propagate away from impact centre. Circumferential cracks then form within these radial cracks. Circumferential cracking demonstrates the amount of flexing in the body and form in families of concentric circles. Significantly impacts ballistic performance for subsequent strikes.

To summarise, the forces induced during high-velocity ballistic impact are through-thickness compression and shear. These are followed by three-dimensional bending of the target creating membrane stretching. The design considerations for the failure modes in Table 7 are described below in Table 8.

Table 8: Multilayer Armour Penetration Mechanism Design Considerations [10]

Mechanism	Design Consideration
Delamination	The propagation of delamination cracks is governed by the resin's fracture toughness. Therefore, a high-interlaminar shear strength preferred.
Discing	The interlaminar shear cracks are governed by the in-plane elastic modulus and the through-thickness strain to failure. The interlaminar fracture toughness governs then governs the delamination cracking and discing.
Radial and Circumferential Cracking	Sherman reported that radial cracks are driven through the generation of hoop stress at the impact centre. Therefore, the magnitude of the tensile hoop stress and the fracture mechanics of the material governs radial cracking. A study by Elder found one radial crack per approximately 150MPa of developed hoop stress. Circumferential cracking is governed by the support provided to the brittle material via a backing material. The greater the support, the lower the bending moment along the radial direction of the body propagating cracks.

3.6 Analysis of Existing Ballistic Protection

3.6.1 Small Arms Protective Insert - BAE Systems

The small arms protective insert (SAPI), developed by BAE Systems, is a hard armour plate (HAP) employed by the United States Army and Marine Corp. Displayed in Figure 3, it is a good representation of the current industry standard of body armour. The plate is constructed using boron carbide or silicon carbide composite. The backing material employed to reduce the collateral damage from the brittle HAP is constructed using Honeywell Spectra Shield fabric [1].

Figure 3: The Small Arms Protective Insert by BAE Systems [1]

In a typical impact scenario, the amour initially shatters and blunts the projectile on the ceramic plate. Hence, this dissipates the kinetic energy into the hard ceramic. The projectile begins to erode as its remaining momentum is dissipated into the backing material (fibre reinforcement). The backing material also captures any ceramic fragments and residual material from the projectile restricting further damage to the wearer. Figure 4 displays a cross section of the standard ceramic armour system.

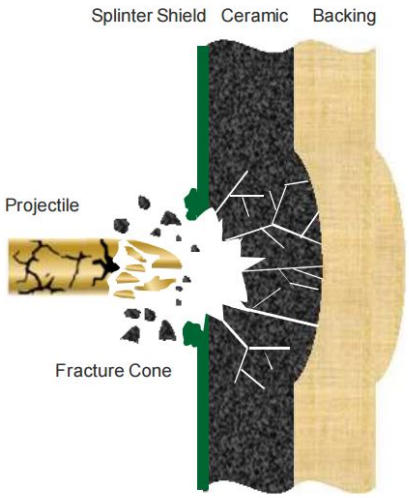

Figure 4: Typical projectile penetration of layered ceramic composite armour [11]

As the primary material is a brittle ceramic, the SAPI has seen numerous improvements due its service life due to its poor multi-hit capacity. The large impact fracture zone of the material hindered the ability of the HAP to maintain its ballistic performance in multi-hit scenarios. The enhancements however increased the weight of the armour systems with the large plate increasing by 0.76kg over its service life [1].

3.6.2 SOV 3000 Dragon Skin - Pinnacle Armor

SOV 3000 Dragon Skin armour was an armour system manufactured by the Pinnacle Armor using silicon carbide ceramic disks. Derived from the dermal armour found in animals in nature, it attempted to depart from the traditional ceramic armour system discussed in section 3.6.1 [21]. Figure 5 displays the armour system.

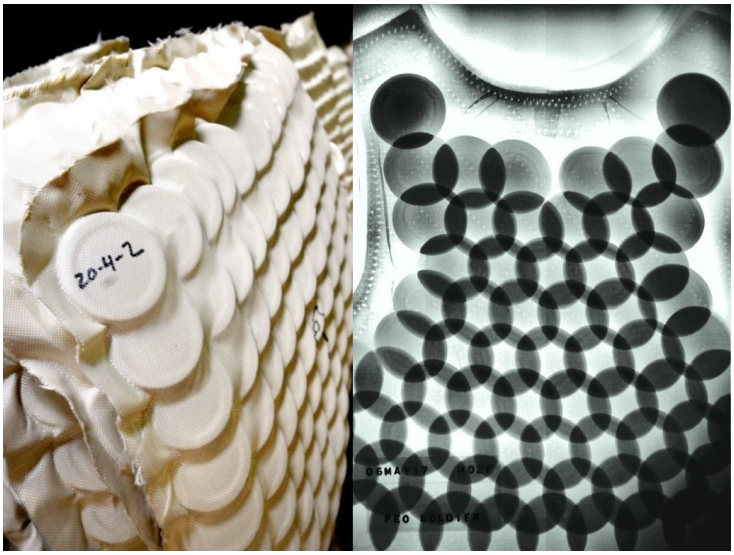

Figure 5: Dragon Skin Body Armour [21]

The system contains overlapped high-tensile SiC disks (two inch diameter) creating a highly-flexible armour. The disks were encased in a glass fibre textile. At normal operating conditions, the armour operated extremely well however it failed when tested at the *conditioned* state. When exposed to the conditioning standards discussed in section 3.2.1, the adhesive used to laminate the discs failed. This hence caused the disks to delaminate and accumulate at the bottom portion of the vest. Further, Dragon Skin armour was deemed to be approximately 9 kg heavier than the in-service SAPI armour during the time of testing [17].

3.7 Fibre Reinforcement in Armour Panels

Research into the effects of energy-absorption due to ply undulations are in its infancy. However, undulations at the fibre level has seen significant research in recent years. This chapter will discuss current fibre reinforcements used in ballistics and upcoming three-dimensional fibre architectures.

3.7.1 Standard Weave Patterns

From the discussion presented in section 3.4, it is apparent that the ballistic resistance is increased by increasing the length of the fibre. Therefore, within each reinforcement weave pattern, the weaving points act as energy concentrations on impact. As discussed below, there is a fine balance to be achieved between the length of the fabric and the number of weaving points. No weaving points allows a projectile penetrate through the fabric, but a short fibre will fail at dissipating the elastic waves effectively on impact.

Chu et. al [8] conducted a detailed analysis into the performance of standard weave patterns in ballistic impacts. The analysis compared the performance of plain, satin, twill and basket weaves. A 1/1 plain weave was found to be the best performing pattern and this was credited to the stability of the fabric construction. While there was sufficient inter-fibre motion (which aids energy dissipation), the friction between the fibre hindered the projectile from penetrating through the fabric.

Even with longer fibre lengths, satin weaves were found to have very poor ballistic resistance due to the low amount of warp-weft fibre interweaving. Rather, the plain and twill patterns outperformed at lower velocities (<400 m/s) due to the higher density of warp-weft interweaves. In high velocity impacts, basket weaves provided the highest level of ballistic resistance. Figure 6 displays the 4 weaving patterns discussed.

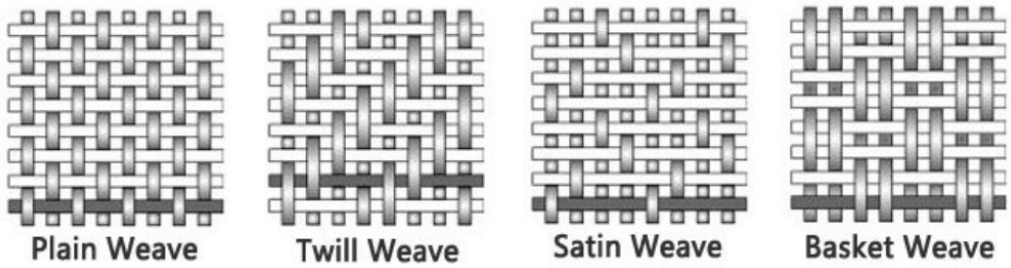

Figure 6: Standard Weave Patterns [**?**]

3.7.2 3D Woven Fibre Architectures

There are two key types of 3D woven fibre architectures, those being either fibre-level or ply-level undulations. In an analysis conducted by Henry et. al into material properties due to ply undulations, it was noted that ply undulations were detrimental to the axial compressive modulus and strength of both flexible and rigid matrix composites. The plies tested were

two-dimensional, uni-directional laminated. Unfortunately, this does not directly transfer to energy absorbing panels as it is the transverse compressive properties that are prevalent.

Fibre-level architectures are currently used in aerospace structural applications such as fan blades and landing gear braces [19]. There are two key types of fibre-level architectures, these being orthogonal and angle interlock fabrics.

Orthogonal fabrics, as displayed in Figure 7, provide a fibre architecture which is resistant to composite delamination. In these materials, fibre undulations are achieved by a single warp tow binding the fabric together from the top to the bottom layer. By increasing the binding tows in the weft direction, the resistance to delamination can be increased [7]. Compared to standard two dimensional fabrics, the interlaminar fracture toughness is increased due to the warp yarn binding.

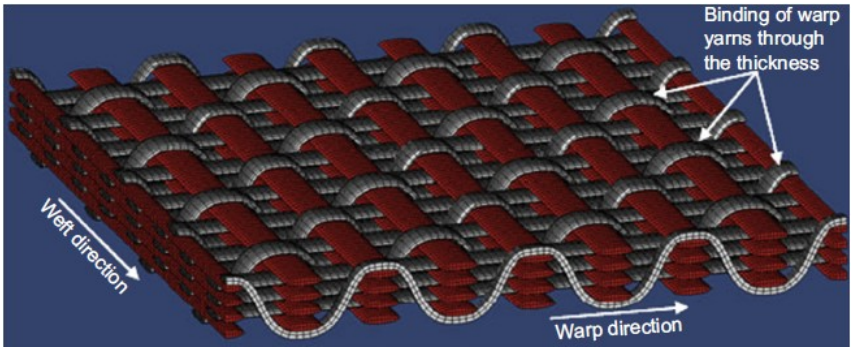

Figure 7: Four-layer 3D Orthogonal Fabric [13]

In an analysis conducted by Ha Ming et. al into numerical modelling of 3D orthogonal structures in ballistic scenarios, an interesting phenomenon was highlighted. The fibre undulations in the fabric caused the transverse strain wave to propagate elliptically as displayed in Figure 8. During impact, the weft tows (straight tows) are completely tensed while the transverse strain wave develops on them. The warp yarns remain in a de-crimping process. Hence, the panel is damaged in the weft direction to the extremities of the body while the damage is restricted in the warp direction. This phenomenon highlights the potential of orthogonal fabric structures to have high ballistic performance in multi-hit scenarios. However currently, the complexity of the fabric structure decreases its manufacturability for commercial production.

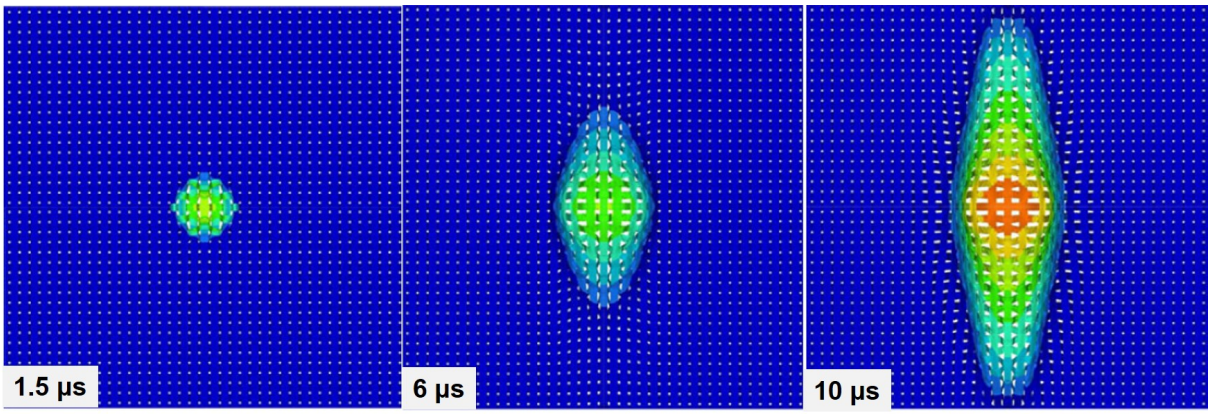

Figure 8: Behaviour of 3D Fabric Upon Impact [13]

Angle-interlock structures are used to increase the tensile modulus and tensile strength in the warp direction. They use fibre undulations through the diagonal weaving of tows in the through-thickness direction. Figure 9 display examples of angle-interlocking fibres. However, these fabric structures have a low shear modulus, increasing its moldability. Currently these fabrics are being researched for use in female ballistic body armour due to this characteristic [7].

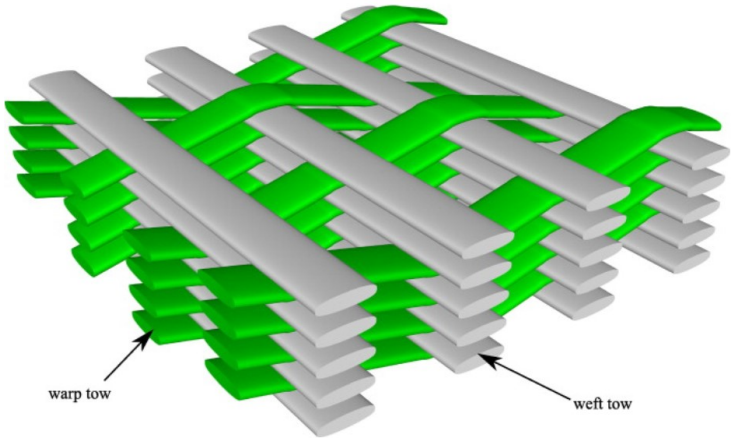

Figure 9: Angle-Interlock Fabric Structure [19]

As expressed by Boussu in his analysis into the angle-interlock fabric in ballistic impact, the structure displayed high strength and damage resistance due to the weft and warp fibre interlace. Additionally, observations were made into the localised delamination of the material at point of impact compared to uncontrolled circumferential delamination observed in standard weave patterns.

4 Experimental Methodology

This study used an iterative process to converge to a more refined result. The flowchart displayed in Figure 10 displays the basic structure of the methodology used.

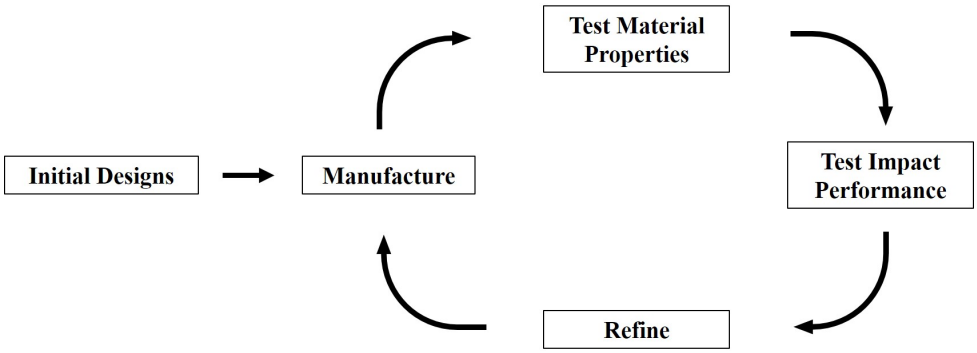

Figure 10: Experimental Methodology

After the initial undulation patterns were designed, they were manufactured using glass fibres. Glass fibres were able to be readily sourced as it was relatively inexpensive compared to Aramid. Hence, glass fibres were used for the vetting process for the undulation designs and manufacturing methods. During each batch of sample manufacturing, a reference sample was also manufactured which emulated a standard ply layup used in industry. Figure 11 displays this layup sequence and each reference sample corresponded to the same thickness and material of each batch. Tthe performance of the undulation designs were compared against the performance of the corresponding reference sample.

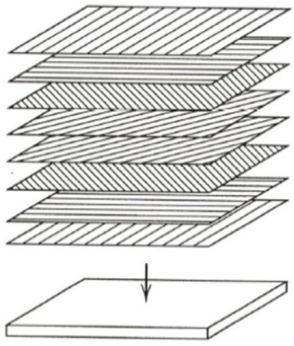

Figure 11: Industry layup sequence for body armour

The performance of each design was tested via material and ballistic impact testing. As expressed before, the impact testing was a simulation of a ballistic impact scenario. Therefore, each sample was mounted against a block of ballistic gel which simulated the human body. From the gel, the penetration depth and any effects due to spall were noted.

5 Undulation Designs

This chapter presents the fibre undulation designs used in this study. Each undulation design was drafted using the considerations extracted from the literature survey. All stitching of any material (detailed in manufacturing) was done using a plain cotton string (stitches indicated in red). Table 9 details the initial undulation designs.

Table 9: Preliminary Fibre Undulation Patterns

Design Code	**Design**	**Remarks**
LI	*Layer-Interlock* 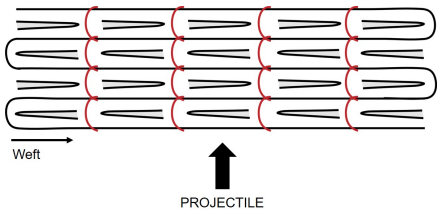	Single undulating interlocking ply (maximised fibre length). Increased chance of delamination due to slip. Cotton stitch will require reinforcement dissipate energy better.
L	*Layered* 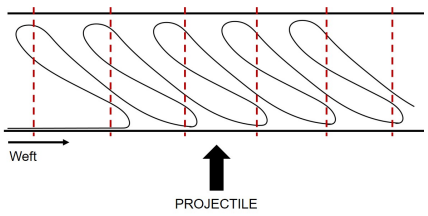	Inspired by the *Dragon Skin* armour analysed in the literature review. Minimum five layers at any one point therefore minimises energy concentrators. Each undulation 15 mm wide.
RO	*Rolled* 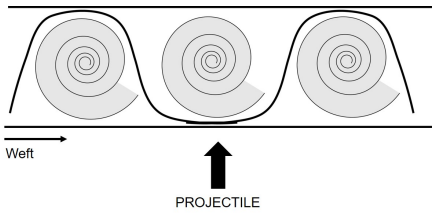	Rolled fabric interlocked with weft ply. The area between the rolls of fibre will be matrix dominated and may act as energy concentrator. The design increases the fibre length hence aiding ballistic resistance. 20mm wide fibre rolls.
MRO	*Multi-Roll* 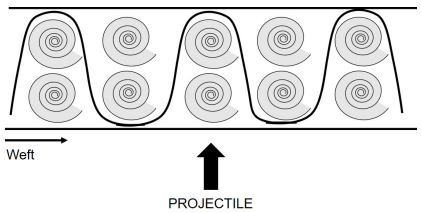	Increased tow mobility in through thickness direction. Potential for unplanned increase in stiffness of panel. 15 mm wide fibre rolls.

Initial testing was limited to designs *L* and *RO*. However, following the initial rounds of testing, the designs were refined to improve the mechanical properties of each structure. These refined designs are presented in Table 10.

Table 10: Refined Fibre Undulation Patterns

Design Code	**Design**	**Remarks**
ML	*Multi-Layer* 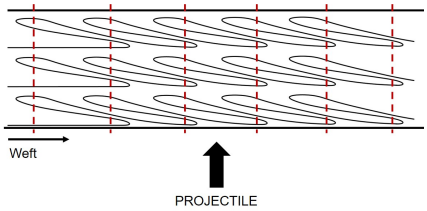	Stacking of layered undulations over each other. Each fibre ply is engaged as projectile *squeezes* through reinforcement.
C	*Combined* 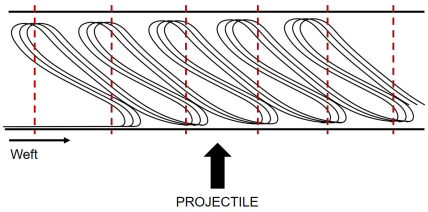	Inspired by basket weave and its improved performance at higher velocities. All plies are engaged on impact, rapidly dissipating the energy.

The key observation in the energy dissipation mechanism of ply level fibre undulations is that energy concentrations are localised to the affected undulations. Therefore, a balance needed to be achieved between the size of each undulation as too narrow undulations increased the stiffness of the panel and wider undulations reduced the ballistic resistance.

5.1 Naming Convention

In order to better explain the manufactured samples, the following naming convention has been adopted.

Design Code (Sample Number) - Material - Sample Thickness - Fibre Volume Fraction

For example, ML(1)-A-3-78 indicates the first sample of the multilayer undulation design constructed using Aramid fibres. The sample is 3 mm thick and contains a 78% fibre volume fraction. The design code for the reference samples manufactured is *REF*.

6 Manufacture

6.1 Sample Manufacture

The composite laminates were manufactured using wet-layup with curing under the compression of a press or vacuum bagging. While vacuum bagging provided a greater consistency of resin infusion into the matrix, there was limited scope for controlling the thickness of the samples. Hence, while vacuum bagging was initially utilised for the curing process, the press was utilised for curing the Aramid samples which improved the consistency of sample thickness. In the subsequent sub-sections, the manufacturing process will be detailed. Sample manufacture was conducted in the following order:

1. Prepare ply level undulation using cotton stitching
2. Layup fibre reinforcement with epoxy matrix
3. Cure under vacuum or press
4. Use water-jet precision cutter to cut samples to size

6.1.1 Fabric Preparation

Depending on the target undulation, different ply sizes were cut and stitched for manufacture. Table 11 presents the material required to prepare a 100 mm $\times$ 100 mm $\times$ 4.5 mm sample using 0.3 mm thick fibre. A tolerance of 10 mm was added to each side to account for manufacturing inconsistencies and mounting area for the water-jet cutter.

Table 11: Material Requirement for 4.5 mm Thick Samples (using 0.3 mm thick fibre)

Design Code	**Target Undulation Specification**	**Required Fabric Sizing**
REF	Nil undulation	• 15 $\times$ 120 mm $\times$120 mm
ML & C	15 mm wide undulation	• Undulation - 3 $\times$ 600 mm $\times$120 mm • Face Sheets - 2 $\times$ 120 mm $\times$120 mm
RO	20 mm wide roll	• Rolls - 6 $\times$ 240 mm $\times$120 mm • Interlock ply - 1 $\times$ 300 mm $\times$120 mm • Face Sheets - 2 $\times$ 120 mm $\times$120 mm

Note, Aramid fibres required significant shearing force to cut through. It was found that very sharp scissors and electronic fabric shearers were best suited for this task. Insufficient cutting tools degraded the edge finish of the fabric and resulted in individual tows being displaced from the weave structure. Figure 12 presents the undulation pattern used for the *C* and *ML* designs ready for layup. A paper model was first created to confirm the sizing of the undulation. In this design, the 15 mm undulation is achieved via a 15 mm offset in each fold. Therefore, the folds in the figure occurred every 30 mm and 45 mm.

Figure 12: Stitched Ply of *C* and *ML* Undulation Designs

6.1.2 Layup and Cure

Once the fabric was prepared for the respective undulation design, it was manufactured using an epoxy resin. The materials used during this process are listed below.

1. Colan 300 gsm twill weave glass fibre
2. Colan 175 gsm plain weave Aramid fibre
3. West System 105 Epoxy Resin
4. West System 205 Hardner
5. West System 206 Hardner

The key material properties of the fibres and resin are presented in Tables 12 and 13.

Table 12: Colan Reinforcement Fibre Properties [9]

Material	**Density (g/m^2)**	**Tensile Modulus (GPa)**	**Tensile Strength (MPa)**
Glass	300	87	4600
Aramid	175	124	3600

Table 13: Colan Reinforcement Fibre Properties)

Resin/Hardner	**Tensile Modulus (GPa)**	**Tensile Strength (MPa)**
105/205	2.8	54
105/206	3.2	50

The cure characteristics for the two different hardners are presented in Table 14. As the 206 Hardner had a slower gel time, it was used for the designs which took longer to wet out. These were *RO* and *C* designs.

Table 14: West System 105 Epoxy Resin and 205/206 Hardner Cure Characteristics)

Hardner	**Pot Life (min)**	**Cure Time (hr)**	**Minimum Temperature (°C)**
205	9	12	10
206	20	17	16

The ratio between the hardner and resin is one part hardner to five parts hardner. Enough resin was prepared to achieve a fibre volume fraction of 70%. The layup process involved wetting each ply and stacking them in sequence as per each design. Figure 13 displays the layup for RO samples.

Figure 13: Layup of *RO* Samples

Once each full stack was wetted out, the sample was placed in a Teflon film vacuum bag. A vacuum pump operating between -80 to -100 kPa was then utilised to pull vacuum through the bag. It was imperative that the pump was operating at the correct pressure to ensure all excess resin is pulled out of the sample.

Following the initial rounds of manufacture, the vacuum bagging was replaced with the use of the hot press during cure. Utilising 4.25 mm spacers, the samples were pressed down once the layup was complete achieving a superior consistency in the sample's thickness. Note, the hot press was only utilised for it's press functionality and no heat was applied during the pressing. A 15 kg clamping force was applied by the press. Figure 14 shows the press in operation clamping a stack of four laminates.

Figure 14: Pressing of Aramid Layup Using Press

6.1.3 Finishing

Once the samples were cured, they were sized using the precision water-jet cutter available at University of Queensland's civil engineering structures laboratory. The samples had a manufacturing tolerance of $\pm$ 3 mm on each side ($\pm$ 6 mm total). This tolerance was derived as the clamping mechanism of the sample for impact testing required a minimum of 6 mm on each side for a secured fit. However, for a 6 mm thick sample, the water-jet was within $\pm$ 0.5 mm.

Figure 15 displays manufactured Aramid samples.

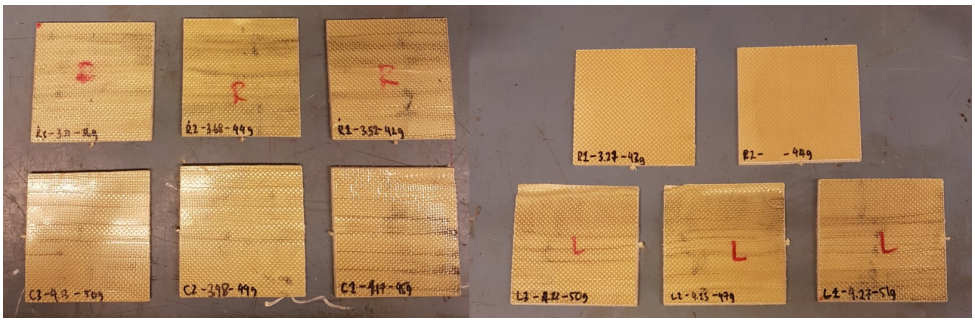

Figure 15: Manufactured Aramid Samples

For the glass fibre samples, the material testing specimens were cut using a diamond tipped trim saw as displayed in Figure 16. Aramid samples required the water-jet as the cutter was inadequate.

Figure 16: Cutting Glass Fibre Material Testing Specimens

6.1.4 Volume Fraction Calculation

The volume fractions for the completed samples were approximated using the mass fractions. With the glass fibre samples, the vacuum bagging removed all excess resin to the breather cloth, hence the error in the volume fractions calculated using this method was minimised. This was apparent as the fibre volume fractions were only $\pm$ 3% from the target fibre volume fraction.

This same method was not applicable to the Aramid samples. During the curing of the sample using the press, the excess resin was squeezed to the edges of the samples. Therefore, the excess resin was still part of the sample and was only removed once the samples were cut to size using the water-jet. Initial fibre volume fractions calculated indicated 55% with the target

fibre volume fraction of 70 %. Therefore, to better approximate the volume fractions, a simple calculation was conducted using th e approximate areal weight of the fabric used in each design and the finished water-jet samples.

6.2 Ballistic Gel Manufacture

As discussed previously, ballistic gel was manufactured acting as the backing layer of each sample during impact testing. The key consideration when manufacturing the gel was to ensure that the correct density was achieved to ensure that it accurately modelled the density of human flesh.

The materials used to make the gel are presented in Table15. The following material list produces 7 L of ballistic gel given that the ratio used for achieving the correct density of gel is one part gelatin to six parts water.

Table 15: Ballistic Gel Manufacture Materials

Item	Quantity	Remarks
8L Storage Container	1	Acts as the gel mould. Adjust size depending on required gel dimensions and volume.
Food-grade Unflavoured Gelatin	1 kg	
Hot Water	6 L	Ensure water is not boiling. Ideal temperature is 60 °C ± 5 °C.
Propionic acid	5 ml	Used to stabilise gel and prevent mould. Essential if gel is going to be used multiple times.
Silicon Grease	20 g	Used as release agent for removing gel from container. Can be substituted with other lubricants.
Spatula	1	Can be substituted with any mixing utensil.
Large Mixing Bowl	1	Ensure bowl/container is large enough to fit complete mixture of gelatin and water.

The process for manufacturing the gel is presented in the list below.

1. Slowly mix gelatin and hot water in mixing bowl. Add roughly 250 g of gelatin at a time ensuring that the powder is mixed thoroughly.
2. Measure 5 ml of Propionic acid and add to mixture. Keep note of the necessary safety requirements when dealing with this acid. This step can be avoided if the gel will not be reused over a period of time.
3. Continue to mix gelatin thoroughly. Keep note of any powder ”clogs” at the bottom of the mixing bowl which need to be dissolved prior to curing.
4. Remove any foam that may have been created during the mixing process.
5. Prepare the gel mould using a light layer of silicon grease.
6. Gently pour the mixture into the mould. Control the pace of pouring to minimise any foam that may form.
7. Store the gel in a fridge between at 3 °C $\pm$ 1.5 °C.

Figure 17 displays the ballistic gel block which was manufactured. Table 16 presents the properties of the block.

Table 16: Ballistic Gel Properties

Dimensions (l x w x h)	**Mass**	**Density (kg/m^3)**
200 x 330 x 440	5.485 kg	1.2

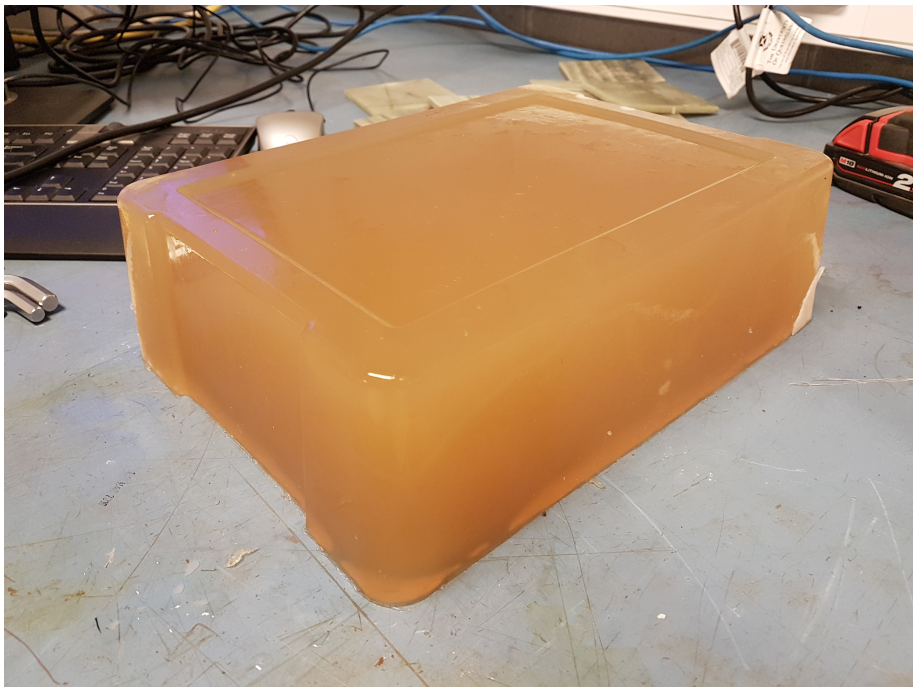

Figure 17: Ballstic Gel Block

6.3 Cannon Sabot Manufacture

The impact testing required a sabot to carry the projectile through the barrel. A 49 mm sabot was cut using the water-jet which fit into the 52 mm barrel of the cannon. The material used for the sabot was a high density polyurethane foam. Once the sabots were precision cut, they were then machined using a drill press to seat the projectile. The fit between the projectile and the foam was a friction fit. Figures 18 and 19 display the boring of the sabots and the completed sabots with the projectile seated in.

Figure 18: Boring of Cannon Sabots Using Drill Press

Figure 19: Completed Cannon Sabots

6.4 Manufacturing Constraints

The key manufacturing constraints encountered during this process have been detailed below.

1. **The nexus between vacuum bagging and pressing** – Initially only vacuum bagging was used as it provided a consistent fibre volume fraction once cured. However, undulations required significant clamping force to ensure that it consolidated correctly prior to the resin gelling. Therefore, the press was then utilised to manfuacture thicker samples with increased consistency however with poor control over fibre volume fraction. A method not explored in this study was resin infusion, however any future work in this field should visit this manufacturing process.

2. **Water-jet cutting is prone to delaminating materials** – The notable issue with the water-jet arose from the delaminations which occurred when the jet pierced into the material. As displayed in Figure 20, significant delamination of the reinforcement layers can be observed at the pierce location. This was then negated by ”leading” in onto the sample therefore reducing the material processing defects.

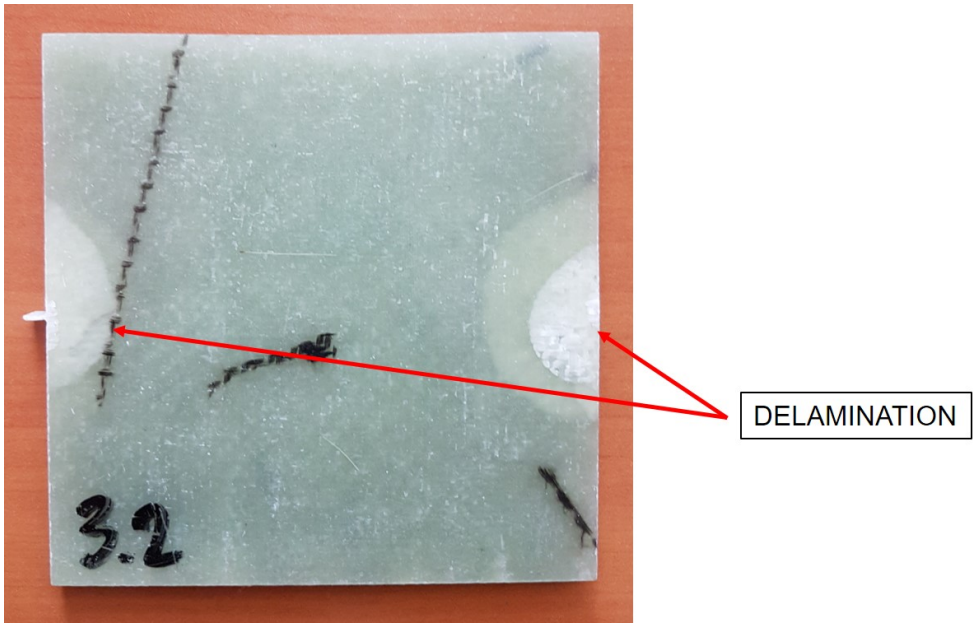

Figure 20: Delamination Caused by Water-jet Cutting

3. **Resources** – Unfortunately, due to the high cost of Aramid, not enough material was able to sourced for manufacture of undulation designs at thicker sample sizes. Ideally, sample thickness would need to be in vicinity of 5 mm in order to provide robust ballistic resistance for low velocity projectiles.

7 Material Characterisation

The material properties of the samples were determined via four-point bend testing as per the ASTM 6272 - 17 Standard Test Method. The method details the process for determining the flexural properties of unreinforced and reinforced plastics via four-point bending. Due to the manufacturing defects and inconsistencies in the samples, it was determined that four-point bending provide more reliable material properties compared to a standard three-point test. It must be noted that the rupture modulus and mechanical strength via the four-point bending test procedures are lower than the properties extracted from a three-point bending test.

The Instron 4505 machine coupled with Bluehill data collection software was utilised for carrying out the four-point test. Figure 21 displays the test machine and a specimen being tested.

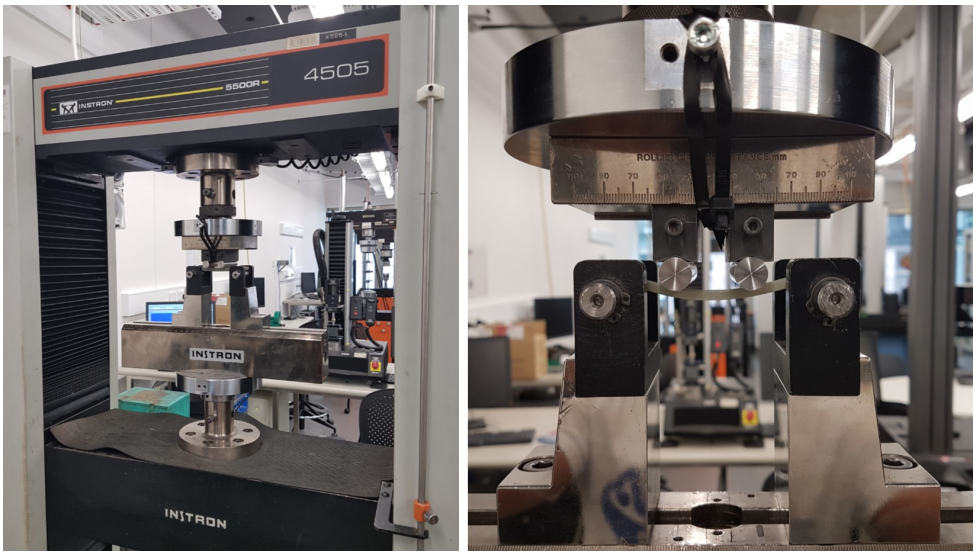

Figure 21: Instron 4552 used for Four-point Bending

From the samples prepared for impact testing, material specimens were prepared as per the ASTM standard. Table 17 presents the specimen specifications and testing conditions. Note, the loading points along the sample was one third of the support span apart as displayed in Figure 22.

Table 17: Four-point Bending Specimen and Testing Properties

Dimensions (mm)	**Span Length (mm)**	**Load Cell (kN)**	**Thickness (mm)**	**Cross Head Speed (mm/min)**
100 x 15	80	10	< 3.2	3
			> 3.2	2

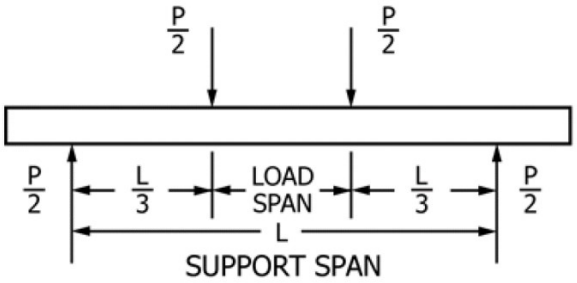

Figure 22: Four-point Bending Loading Points

A minimum of three observations were made for each sample. Figure 23 presents the glass fibre specimens used for the testing. The top nine specimens are the initial manufacturing round and the bottom are from the second. The reference samples are the left most samples from each batch.

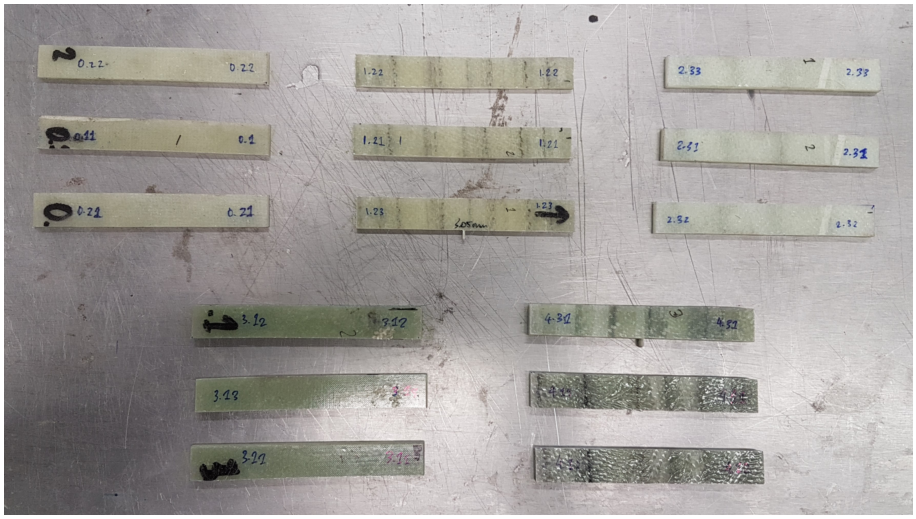

Figure 23: Glass Fibre Material Testing Specimens

Figure 24 displays the Aramid specimens ready for testing. Note, undulation designs ML, C and RO were tested using Aramid.

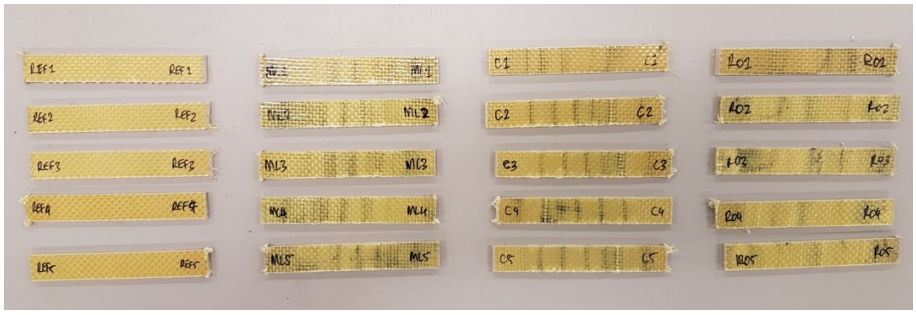

Figure 24: Aramid Material Testing Specimens

The Bluehill software captures the flexure extension of the specimen and the corresponding

loads. From this data, the flexural strength and modulus of elasticity in bending of each material sample was calculated. Equations 3 and 4 present the calculations for flexural strength and modulus of elasticity respectively.

$$\sigma_b = \frac{P_{max} L}{bd^2} \tag{3}$$

$$E_b = \frac{0.21 L^3 m}{bd^3} \tag{4}$$

Additionally, the theoretical laminate modulus was calculated using the micro-mechanics approach of rule of mixtures. Equation 5 presents the rule of mixtures for finding the modulus of a laminate. The key assumptions when calculating the rule of mixtures are as follows.

1. The fibres and matrix are perfectly bonded
2. The distribution of fibres are uniform
3. The matrix does not contain any voids
4. Analysis is linear-elastic

$$E_c = E_f V_f + E_m V_m \tag{5}$$

7.1 Material Properties

Tables 18 and 19 detail the material properties for glass-fibre specimens for the first two batches of manufacture. The data presented is an average over three specimens from each design.

Table 18: Glass-fibre Material Properties - Batch 1

Sample	**Theoretical Modulus (GPa)**	**Flexural Modulus (GPa)**	**Flexural Stress (MPa)**
REF - G - (3.3 $\pm$ 0.1) - 72	63.4	26.9	488.7
ML - G - (2.83 $\pm$ 0.3) - 69	60.9	20.1	262.9
RO - G - (3.86 $\pm$ 0.1) - 68	60.0	20.5	130.4

Table 19: Glass-fibre Material Properties - Batch 2

Sample	**Theoretical Modulus (GPa)**	**Flexural Modulus (GPa)**	**Flexural Stress (MPa)**
REF - G - (5.82 $\pm$ 0.33) - 67	59.3	21.2	390.3
C - G - (5.63 $\pm$ 0.19) - 71	62.7	17.9	158.3

From analysing the data, it was evident that the mechanical properties of the undulated samples were lower than the reference samples. This was in line with the study conducted by Henry et. al into the effects of ply level undulations on mechanical properties. The key consideration drawn from the material testing was that the undulated samples did not exhibit ultimate failure as rapidly as the reference samples. For example, if design ML, once one layer failed, it would transfer a great load onto the next fibre layer and maintain basic mechanical integrity.

Further, unavoidable premature failure was observed in some samples due to manufacturing defects such as that displayed in Figure 25.

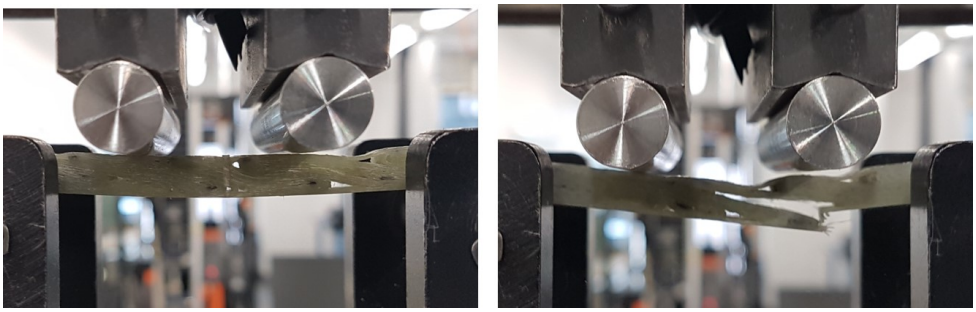

Figure 25: Premature Failure of Testing Specimens

Table 20 details the properties of the Aramid samples.

Table 20: Aramid Material Properties

Sample	**Theoretical Modulus (GPa)**	**Flexural Modulus (GPa)**	**Flexural Stress (MPa)**
REF - A - (3.38 $\pm$ 0.1) - 66	82.8	26.5	188.1
C - A - (4.15 $\pm$ 0.1) - 62	77.9	16.2	129.1
ML - A - (4.45 $\pm$ 0.1) - 64	80.4	19.0	136.5
RO - A - (3.59 $\pm$ 0.1) - 61	76.7	13.6	85.6

8 Ballistic Impact Tests

The University of Queensland's composite group maintains a pneumatic cannon commissioned for impact testing projects. The cannon is vertically aimed and was able to projectiles at over 200 m/s. A schematic of the impact test setup is displayed in Figure 26.

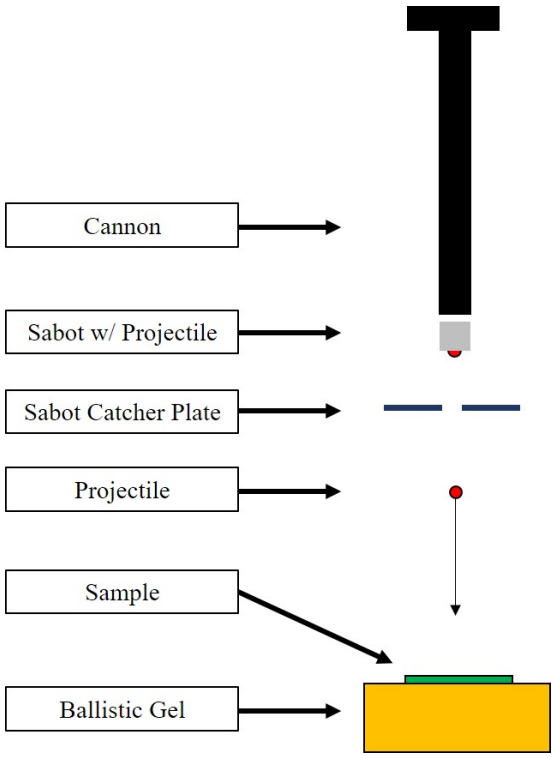

Figure 26: Impact Testing Setup

The projectiles fired out of the cannon were ball bearings. During initial testing, a larger projectile was used weighing 10 g and 12 mm in diameter. However, the projectiles were limited to velocities between 120 - 160 m/s. In order to better improve projectile velocity, a smaller projectile of 5 g and 10 mm diameter was utilised. The projectiles were spray painted white to increase their visibility in the impact footage. Figure 27 displays the projectiles used.

Figure 27: 12 mm and 10 mm Projectiles Used for Impact Testing

The primary data collection tool during the impact testing was a Photron Fastcam UX100. The camera captured the ballistic impact event at 25000 fps. The footage was then analysed using the Photron Fastcam Analysis software package to obtain the impact and rebound velocities. Figure 28 shows a screen shot of the software tracking the projectile and calculating the velocity.

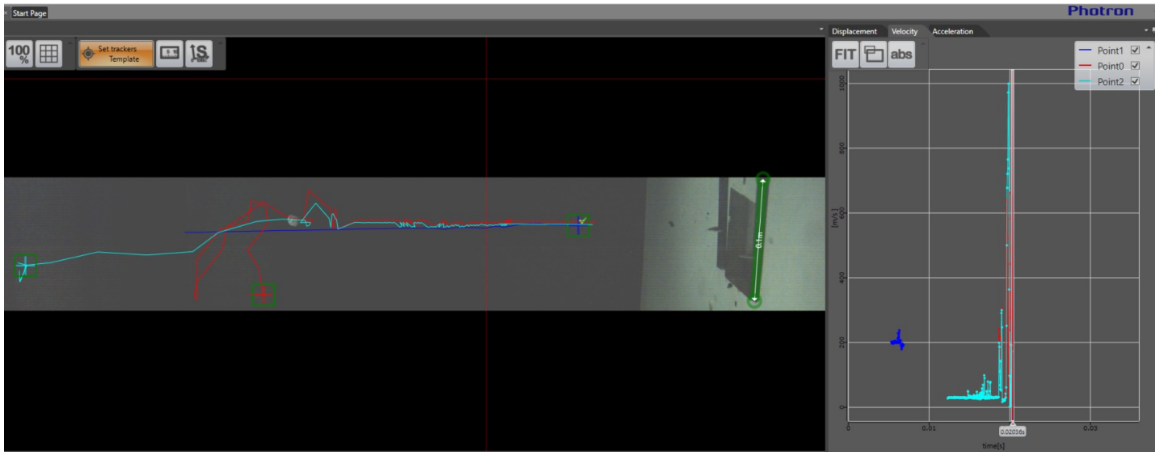

Figure 28: Photron Fastcam Analysis Software Tracking Projectile Velocity

Once impact and rebound velocities were determined, the corresponding energy was calculated using equation 6 (kinetic energy).

$$KE = \frac{1}{2}mv^2 \tag{6}$$

8.1 Glass Fibre Samples

As highlighted by Behera et. al [2] in their analysis of the mechanical behaviour of 3D woven composites, many glass-fibre laminates are translucent in nature. Therefore, when impacted, the damaged regions turn opaque allowing the observer to easily determine the dissipation of energy within the sample. A majority of this damage represents delamination within the laminate. Table 21 details the impact data conducted on the preliminary glass fibre reinforced samples. These samples were impacted using the 12 mm projectile.

Table 21: Glass-fibre Ballistic Impact Test Results - Batch 1

Sample	**Impact**	
	Velocity (m/s)	**Energy (J)**
REF - G - 3.3 - 72	156 ± 2	146.0
ML - G - (2.83 ± 0.3) - 69	149 ± 4	133.2
RO - G - (3.86 ± 0.1) - 68	167 ± 2	167.3

Figure 29 displays the energy absorption and delamination profiles of the two undulation designs compared to the reference sample. The samples have been illuminated to better highlight these profiles.

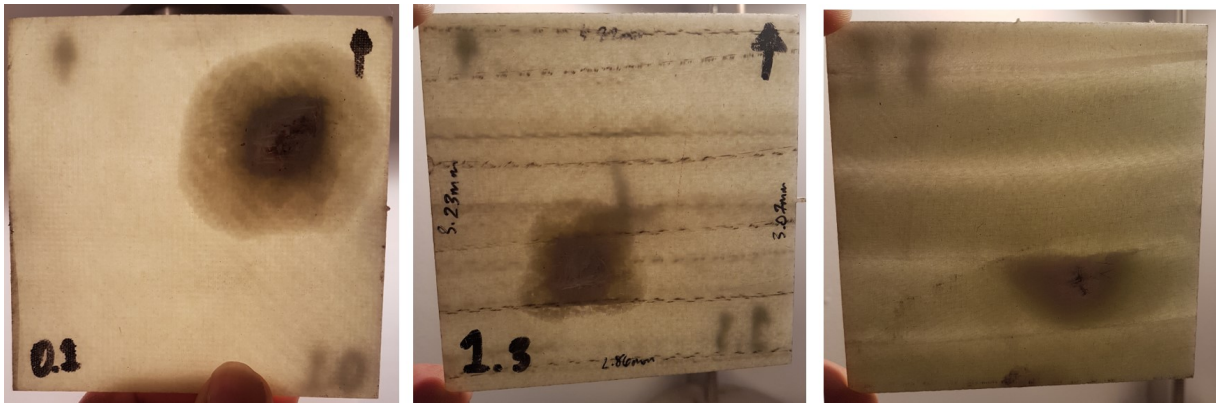

Figure 29: Energy Absorption and Delamination Profiles of Glass Samples - Batch 1 (REF, ML, RO designs)

The energy dissipation profile in each of these samples are profoundly different. Within the reference sample, the energy dissipated circumferentially while within ML and RO designs, the dissipation was localised along the undulations. In RO, it was evident that the single fibre roll which was directly engaged upon impact absorbed a majority of the energy. Within ML, even though the undulation is only 15 mm wide, there is a minimum of 45 mm of fabric folded underneath to support each undulation. Therefore, the ballistic performance about the impact area is superior compared to the other designs.

Table 22 presents the data for the second batch of glass-fibre samples manufactured. These samples had an increased sample thickness to improve ballistic resistance.They were also the first to be tested with the smaller 10 mm projectile.

Table 22: Glass-fibre Ballistic Impact Test Results - Batch 2

Sample	**Impact**		**Rebound**		**Percent Energy Absorbed**
	Velocity (m/s)	**Energy (J)**	**Velocity (m/s)**	**Energy (J)**	
REF(1) - G - 5.96 - 67	202 $\pm$ 6	81.6	32 $\pm$ 2	2.1	97.5
REF(2) - G - 5.91 - 67	203 $\pm$ 3	82.42	30 $\pm$ 2	1.8	97.8
REF(3) - G - 5.83 - 66	199 $\pm$ 6	79.2	38 $\pm$ 5	2.9	96.3
ML(1) - G - (5.77 $\pm$ 0.3) - 71	197 $\pm$ 3	77.62	20 $\pm$ 1	0.8	98.9
ML(2) - G - (5.83 $\pm$ 0.2) - 72	201 $\pm$ 3	80.8	4 $\pm$ 1	0.03	99.9
ML(3) - G - (5.82 $\pm$ 0.3) - 71	200 $\pm$ 4	80	24 $\pm$ 1	1.2	98.6

This round of testing did not have any penetrations through the samples. The test utilised thicker samples but smaller, faster projectiles. From the data, it is clear that the undulated ML design absorbed more energy than the corresponding reference sample. ML(2) is of particular interest as it was able to absorb 99.9% of the impact energy while resisting penetration. Figure 30 displays this sample.

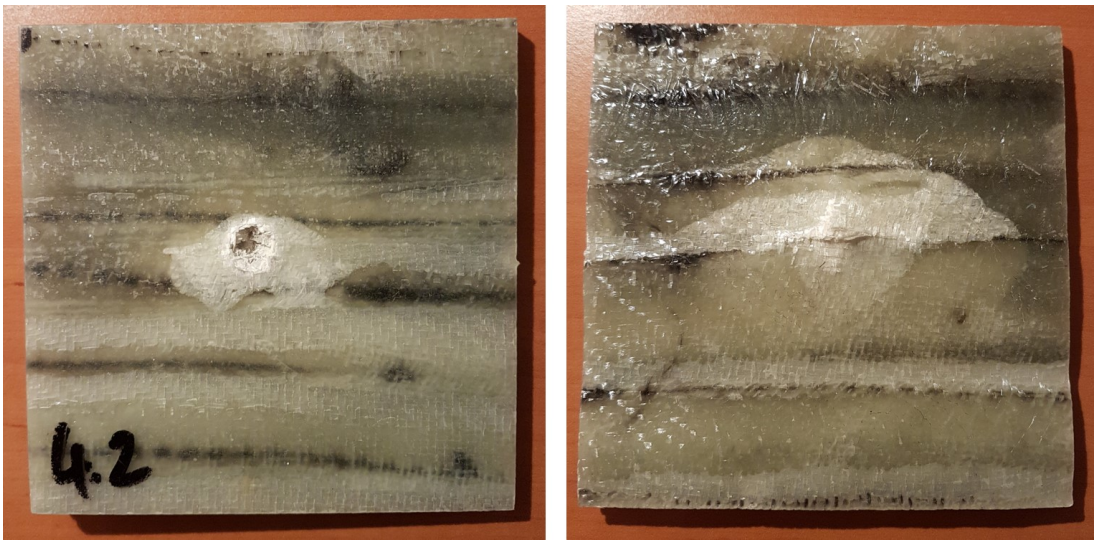

Figure 30: *ML(2) - G - 2.7 - 66* Impact

8.2 Aramid Samples

Table 23 details the testing data for the Aramid samples.

Table 23: Glass-fibre Ballistic Impact Test Results - Batch 2

Sample	Impact		Rebound		Percent Energy Absorbed
	Velocity (m/s)	Energy (J)	Velocity (m/s)	Energy (J)	
REF(1) - A - 3.27 - 66	200 $\pm$ 4	80.0	25 $\pm$ 2	1.25	98.4
REF(2) - A - 3.24 - 66	201 $\pm$ 2	80.8	-	-	-
ML(1) - A - 4.27 - 64	197 $\pm$ 2	77.6	-	-	-
ML(2) - A - 4.23 - 64	203 $\pm$ 2	82.4	16 $\pm$ 1	0.5	99.4
ML(3) - A - 4.22 - 64	204 $\pm$ 4	83.2	12 $\pm$ 2	0.3	99.6
C(1) - A - 4.17 - 63	201 $\pm$ 1	80.8	-	-	-
C(2) - A - 4.23 - 62	200 $\pm$ 2	80	-	-	-
C(3) - A - 4.13 - 62	204 $\pm$ 2	83.2	-	-	-
RO(1) - A - 3.52 - 60	203 $\pm$ 2	82.4	-	-	-
RO(2) - A - 3.68 - 61	198 $\pm$ 4	78.4	-	-	-
RO(3) - A - 3.21 - 61	203 $\pm$ 4	82.4	-	-	-

The behaviour of Aramid samples displayed some differences compared to the glass fibre samples. Referring back to the ballistic impact dynamics discussed in section 3.3, it was noted that the velocity of the stress wave increases with a crease in bulk density but increase in elastic modulus. Compared to glass fibre, Aramid fibres possess both a lower bulk density and elastic modulus. Therefore, the material was more suited for ballistic impacts.

While a majority of the samples did fail due delamination and discing, four samples were able to resist penetration. For example, *C(1) - A - 4.17 - 63* was able to completely arrest the projectile within the weave as displayed in Figure 31. The projectile impacted perfectly normal to an undulation and therefore engaged each ply to dissipate the energy.

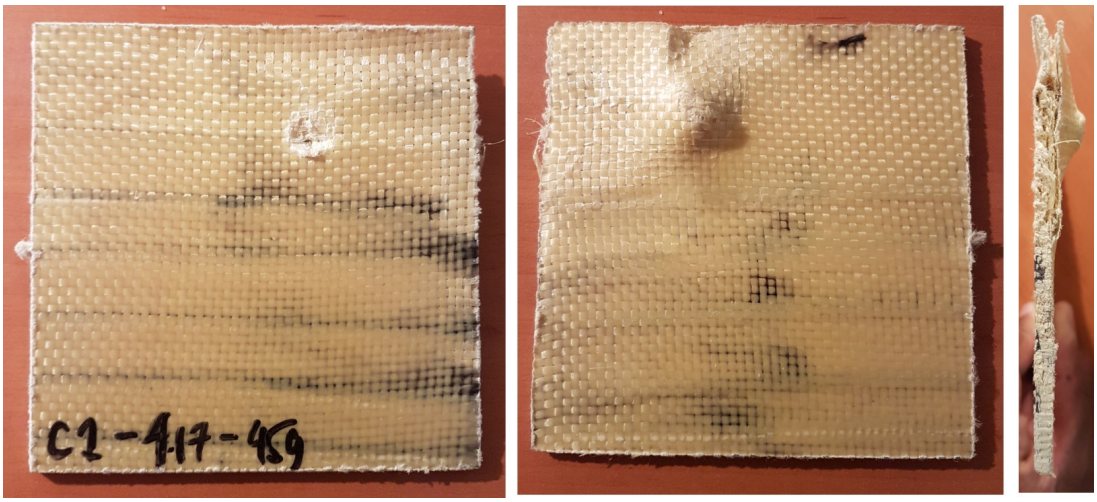

Figure 31: *C(1) - A - 4.17 - 63* with Arrested Projectile

The RO designs demonstrated poor ballistic resistance during the testing. Figure 32 displays the common failure mode of the design. On impact, due to the lack of a robust interlocking weave structure, the rolls of fabric fail quickly in the direction normal to the plane.

Figure 32: Impact Test of *RO(1) - A - 3.52 - 60*

The ML designs demonstrated favourable ballistic resistance. As discussed previously, an impact on this design pattern engages one ply at a time. Therefore, it maximises the use of the undulations and the fibre length of each ply prior to transferring the load to the subsequent layer. Figure 33 displays the successful ballistic resistance of this design.

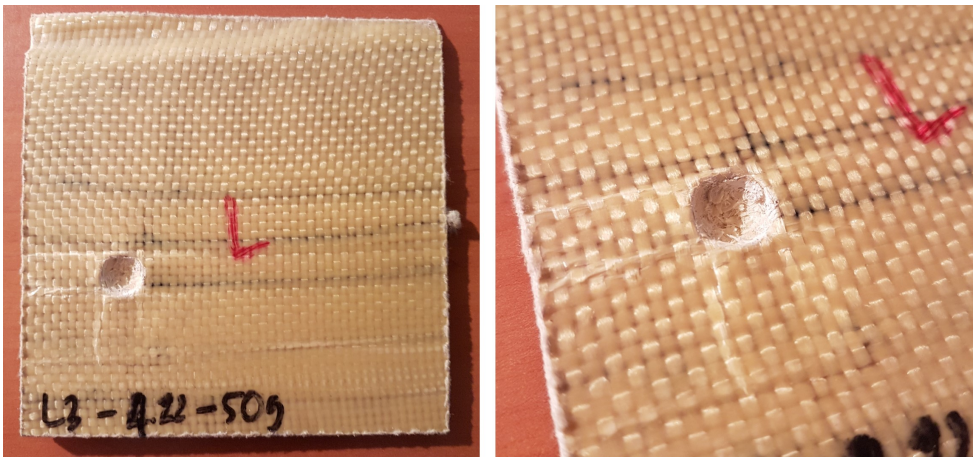

Figure 33: Impact Test of *ML(3) - A - 4.22 - 64*

8.3 Testing Constraints

The ballistic impact testing produced sufficient results for the analysis of energy absorption of each sample. However, the testing apparatus were prone to numerous issues therefore degraded the consistency of data gathering. These constraints are discussed below.

1. **Accuracy of projectile** – A significant issue with the pneumatic cannon was in its difficulty to aim. The barrel could not be reliably aimed to the centre of the sample even after laser adjusting it onto the target. As displayed in Figure 34, very few projectiles impacted the centre of the target.

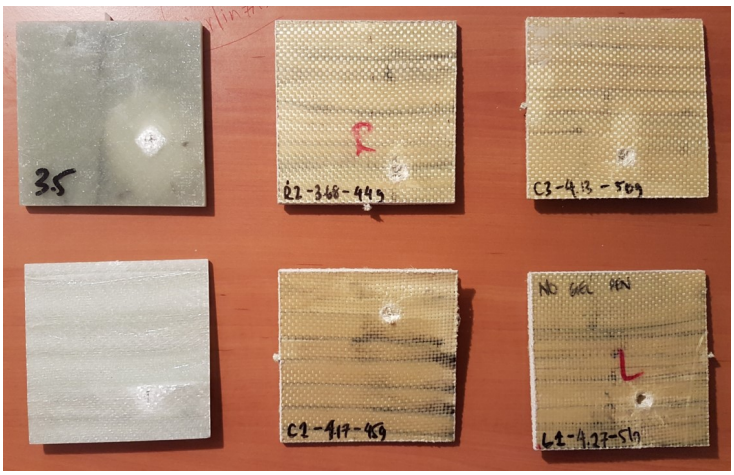

Figure 34: Inaccuracy in Aiming the Cannon

2. **Error in velocity readings** – The projectile was tracked at 25000 fps however, this required a significant amount of lighting and the lighting available was insufficient at times. While the software package tracks the projectile, it does not generate a velocity

reading for the operator. Instead, velocity readings are read off a graph outputting the velocity of the projectile as it moves through the frame. Therefore, the lack of lighting had potential to extrapolate into inaccurate velocity readings.

3. **Pressurised air inlet** – The compressed air for the cannon was supplied by the centralised pneumatic system within UQ's Advanced Engineering Building. There was significant losses in the inlet pressure observed during peak times and hence the velocity of the projectile was slower during these times.

4. **Observation of impact event** – Unfortunately, due to only one high speed camera being available, the impact of the projectile onto the sample was could not be observed. This footage would have allowed a robust analysis of the stress wave propagation within the panels and the subsequent failure modes.

9 Discussion

9.1 Undulation Design Performance

From the analysis conducted, it was observed that the energy absorption of the undulated designs was different to that of the reference samples. Delaminations were localised to run in the direction of the undulation. This potentially acts as a medium for improving the multi-hit capability of a body armour laminate.

The key failure modes observed during the impact testing were delamination followed by spall. With spall being a precursor to discing, it was evident that the initial delaminations from the impacts caused minor in-plane tensile-tearing fracture in most penetrated samples. As spall is a low-energy absorbing failure mode, full penetration of the projectile supported by significant delamination was common. Further, the projectile velocity was not fast enough to initiate the full effects of discing, which may be accelerated due to weak interlaminar shear strength.

Therefore, in order to quantify the ballistic resistance of each undulation design, Equation 7 was developed. This equation presents a ratio between the original fibre length and final undulated fibre length within the manufactured part. For example, for the ML design, the initial ply length was 600 mm then folded into individual undulations of 15 mm. Therefore, at any point of impact, there was 15 mm of exposed fabric reinforced by 585 mm extra fabric to dissipate the load.

$$Undulation\ Performance\ Ratio = \frac{Original\ Fibre\ Length}{Final\ Fibre\ Length\ in\ Part} \tag{7}$$

Table 24 details this undulation performance ratio for the manufactured undulation designs.

Table 24: Undulation Performance Ratio

Design Code	**Undulation Performance Ratio**
REF	1
C	40
ML	40
RO	12

Using this ratio and the analysis presented throughout, Table 25 presents a summary of the performance of each manufactured undulation design.

Table 25: Tested Undulation Design Summary

Design Code	Design	Remarks
ML	*Multi-Layer* 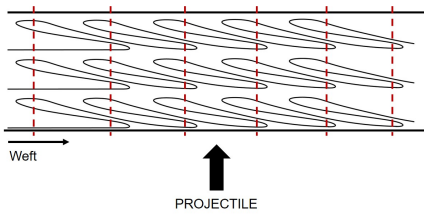	Highest performing undulation design. Dissipated the energy within a highly localised area while only engaging one layer at a time. The design could be improved by off-setting layers to reinforce folding points.
C	*Combined* 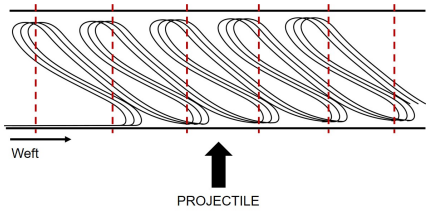	Engaged all fabric in the local impact zone to quickly dissipate the energy. Was susceptible to fibres being drawn out and inducing spall.
RO	*Rolled* 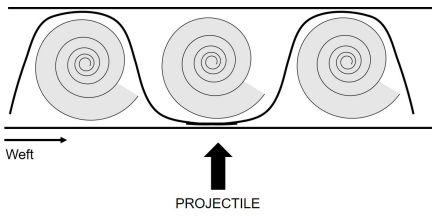	Interlocking fabric was too weak to maintain structural integrity. On impact, the rolled fabric was pushed away from the projectile path allowing it to penetrate through.

9.2 Contributions Made By this Thesis

This thesis made a key contribution to the area of armour materials. It introduced a novel and improved technique for manipulating the energy-absorption in fibre-reinforced laminated materials. Specifically, it developed a fundamental understanding of the energy absorption effects of composite laminates due to ply undulations in low velocity ballistic events. A method to quantify the undulation design performance was also developed.

10 Conclusion

The purpose of this study was to analyse the effects on the energy absorption of a composite armour material due to engineered fibre undulations. The main aims of this study were successfully completed with conclusions drawn on how the energy absorption is affected. Proof-of-concepts were designed and then manufactured. The designs were tested for their mechanical properties and then low velocity ballistic impact testing was conducted to observe the penetration mechanisms and failure modes.

11 Recommendations for Future Work

The field of ballistic protection is dynamic. To continue the work conducted in this study into the future, the following recommendations have been devised.

1. **Improved Ballistic Testing** – In order to improve research value, a robust ballistic impact testing mechanism needs to be developed. The ability to accurately aim the barrel and fire Using such a setup, the effects of fibre undulations due to high-velocity (>800 m/s) impacts can be determined. Until this theory can be validated against a real world threat, it will not gain traction for industrial application.

2. **Numerical Modelling of Ply Undulations** – Currently, there is significant work being conducted into the numerical modelling the performance of 3D fibre architecture under ballistic impact. However, there is limited numerical tools for analysing ply level undulations. A well implemented numerical tool will help remove the guess work when designing fibre undulations.

3. **Improve Fibre Undulation Designs** – The key weaknesses identified in the designs presented in this study can be bolstered by introducing extra reinforcement. Interlocking weaves were not fully explored in this study, however, there is vast potential for interlocking structures within ballistics.

References

[1] BAE Systems (2007). Hard Body Armor Insert Plates. Technical report, Phoenix, AZ.

[2] Behera, B. K. and Dash, B. P. (2015). Mechanical behavior of 3D woven composites. *JOURNAL OF MATERIALS&DESIGN*, 67:261–271.

[3] Brady, C. G. (2003). An Analysis of Wound Statistics in Relation to Personal Ballistic Protection. *Land Operations Division Systems Sciences Laboratory*, pages 1–9.

[4] Bruce, W. (2016). Bullets Explained.

[5] Carey, M. E. (1996). Analysis of wounds incurred by US Army Seventh Corps personnel treated in corps hospitals during Operation Desert Storm, February 20 to March 10, 1991. *Journal of Trauma-Injury Infection and Critical Care*, 40(3):S165–S169.

[6] Cavallaro, P. V. (2011). Soft Body Armor : An Overview of Materials , Manufacturing , Testing , and Ballistic Impact Dynamics Naval Undersea Warfare Center Division. *NUWC-NPT Technical Report 12*, 12(August):1–22.

[7] Chen, X. (2016). *Advanced Fibrous Composite Materials for Ballistic Protection*. Woodhead Publishing.

[8] Chu, C.-k. and Chen, Y.-l. (2010). Ballistic-proof Effects of Various Woven Constructions. 18(6):63–67.

[9] Colan Reinforcement (2017). Fiber Comparison Charts.

[10] Crouch, I. (2017). *The Science of Armour Materials*. Elsevier Ltd, 1st edition.

[11] Fundus, M. (2013). Ballistic Protection Trends In Body Armor and Helmets. Technical report, 3M Technical Ceramics.

[12] Gilat A., Goldberg R.K., and Roberts G.D. (2001). Experimental Study of Strain Rate Sensitivity of Carbon Fibre/Epoxy Composite. In *13 International Conference on Composite Materials*.

[13] Ha-Minh, C., Boussu, F., Kanit, T., Crépin, D., and Imad, A. (2012). Effect of frictions on the ballistic performance of a 3D warp interlock fabric: Numerical analysis. *Applied Composite Materials*, 19(3-4):333–347.

[14] Hazell, P. J. (2015). *Armour: Materials, Theory, and Design*. CRC Press.

[15] Hill, J. L. (2016). Mechanical Property Determination for Flexible Material Systems Mechanical Property Determination for. (May).

[16] Kelly, J. F., Ritenour, A. E., McLaughlin, D. F., Bagg, K. a., Apodaca, A. N., Mallak, C. T., Pearse, L., Lawnick, M. M., Champion, H. R., Wade, C. E., and Holcomb, J. B. (2008). Injury Severity and Causes of Death From Operation Iraqi Freedom and Operation Enduring Freedom: 20032004 Versus 2006. *Journal of Trauma and Acute Care Surgery*, 64(2):S21–S26; discussion S26–S27.

[17] U.S. Department of Defence (2006). Evaluation of Pinnacle Armor SOV 3000 Dragon Skin. Technical Report May.

[18] U.S. Department of Justice (2008). Ballistic Resistance of Body Armor. *NIJ Standard-0101.06*, (August).

[19] Warren, K. C., Lopez-anido, R. A., and Goering, J. (2015). Composites : Part A Experimental investigation of three-dimensional woven composites. *COMPOSITES PART A*, 73:242–259.

[20] Wilusz, E. (2008). *Military Textiles*. Woodhead Publishing.

[21] Yang, W., Chen, I. H., McKittrick, J., and Meyers, M. A. (2012). Flexible dermal armor in nature. *Jom*, 64(4):475–485.